5 Bio-based composite footbridge

Design, production and in situ monitoring

Blok, R., Smits, J., Gkaidatzis, R., Teuffel P. (2019)

Scale 1:1

In the previous chapter the design considerations at the scale of the detail and that of the materialisation is discussed. This chapter addresses bridge design considerations at the scale of the composing materials and their material properties.

This chapter is currently under review in Structural Engineering International (SEI), the Journal of the International Association for Bridge and Structural Engineering (IABSE). Submitted 19 December 2018, accepted for publication with minor revision on 12 March 2019.

Abstract

This paper deals with the design, production and monitoring of a bio-composite footbridge with a span of 14 meters across the river Dommel in the city of Eindhoven, the Netherlands. The specific bio-composite material that was used for this research is a Natural-Fibre Reinforced Bio-Polymer (NFRBP). The goal of the research is to prove that NFRBP can be applied as a load bearing structure in an outdoor environment. For this purpose, a multidisciplinary team of academic researchers from two universities, together with a manufacturer from the NFRBP industry and the Centre of Expertise Biobased Economy (CoEBBE), developed a feasible design that could be produced by unskilled hands in a short period of time and within a limited budget. The footbridge was designed, built and installed within less than one year. In the two years after the installation of the footbridge, the structural behaviour of the bridge was monitored by means of optical fibre glass strands, integrated within the structure, with the purpose of measuring deformations and change in elasticity that occur over time.

Keywords: Bio-based Composites; Bio-based Materials; Circular Economy; Life Time Design; Sustainability.

FIGURE 5.1 The bio-composite footbridge, 18 months after the installation across the river Dommel. R. Blok, J. Smits et al., Eindhoven University of Technology & Delft University of Technology, (2017). Photo by Heijmans (2018).

§ 5.1 Introduction

As the level of impact of global warming and climate change is becoming evident, the search for renewable materials to replace our oil addiction has rapidly gained in urgency. In the field of science the plea for a transition towards a more circular approach of all facets of our economy is gaining in popularity. The necessity of a transition towards a circular economy is especially relevant to the building industry, which of all production industries is depleting our natural and mineral resources with the largest amounts. By way of illustration, at a European level an average of 37.5% of all the wood used is used in construction, 21% of all steel, 65.5% of all glass and 75% of all concrete [1]. That is why a paradigm shift in the building industry towards circular ways of building is unavoidable. In order to meet the ambitions resulting from the Paris Climate agreement it is essential to substantially increase the use of bio-based materials in the building industry [2]. Alternative materials and production techniques need to be found to set off towards a more circular approach. The use of Bio-based materials can be one of a number of different ways towards achieving a more circular economy and a sustainable environment. Furthermore, increasing the use bio-based building materials in the building industry is part of the Dutch National Research Agenda's themes: "Energy and raw materials: Circular economy" [3].

However, so far only a few experimental bio-based building projects have been realised world-wide, either using bio-based materials in non-structural elements such as building facades, or still making partial use of fossil based building materials. To test options for bio-based load bearing structures in the built environment, the authors of this paper have initiated the bio-based footbridge project.

The project aims were to design and build a small, but fully bio-based composite footbridge at the campus of TU/e, and to monitor the service life and degradation in relation to user safety. The project was initiated in November 2015 as a 3TU lighthouse project. The design process started in January 2016 and the bridge was opened by the Alderman of the city of Eindhoven on October 27th 2016. The main load bearing material that has been used to build the footbridge is a bio-composite, for which the scientific name Natural-Fibre Reinforced Bio-Polymer (NFRBP) is proposed. The fibres that were used were partially hemp fibres and partially flax fibres (figures 5.2, 5.4), combined with an epoxy resin that has a 56% bio content (figure 5.3). The non-structural core of the bridge was made out of PLA, also known as polylactide, an aliphatic thermoplastic polyester produced from renewable resources.

FIGURE 5.2 Flax in a field. From https://www.faay.nl/wp-content/uploads/Faay-Wanden-en-Plafonds_Duurzaam-bouwen-met-vlas_vlasveld_3.jpg, visited on 28/02/2019.

a *b*

FIGURE 5.3 Greenpoxy, an epoxy-resin with a 56% bio-content. From a: http://intrey.com/epoksidka/, b: https://www.timeout.de/sicomin-greenpoxy-56-5-kg, visited on 28/02/2019.

FIGURE 5.4 Woven flax fibres. Photo by Dorine van der Linde (2016).

The scope of the project has involved the architectural as well as structural design, the generation, development and selection of design options and the realisation, production and construction of a prototype footbridge of 14 m spanning the Dommel at TU/e campus Eindhoven (figure 5.1). The design follows the requirements in existing codes and standards. A LCA (Life Cycle Assessment) of the bridge as well as a report describing the design steps has been made as part of the project. This paper studies the specific material properties of bio-composites from an architectural as well as structural point of view and discusses the impact of working with bio-composite on the design process.

Furthermore, the research on the structural behaviour of the footbridge over time and under influence of Dutch weather conditions continued for two years after the installation of the footbridge. To this purpose optical Fibre Bragg Grating Sensors (FBG's) have been integrated in the main bio-composite compression and tension zones in order to monitor material strains and deformations.

§ 5.2 Integrated design and project approach

Right from the start of the project, early 2016, small multi-disciplinary teams, comprising architects, bridge designers and structural designers, as well as production experts, started generating preliminary design ideas. These design ideas were reported and discussed in combined design meetings. The resulting most promising ideas have been evaluated on their merits, both architectural and structural as well as from a production point of view and then further elaborated. From these first steps, very early on in the design process, a number of different design principles were formulated:

1 While composite materials can provide a lot of form freedom, the use of a separate mould to shape the bridge through vacuum injection would become too expensive for this project.

2 From early tests it was expected that the preferred combination of resin and fibres would perform better in tension than in compression (creep) therefore a design with relatively low compression stress would have preference.

3 The design would need to be optimised in material use, to keep the production cost sufficiently low while at the same time the aim to create an elegant structural design with a high aesthetical quality should remain an important focus.

§ 5.2.1 Design variations

In the design process, a number of different concepts have been explored. The most promising design alternatives have been further optimised in terms of structural efficiency, structural safety, aesthetical quality, functionality as well as feasibility and cost-effectiveness in production. A main design factor regarding the structural performance of the geometries has been the assumption of higher strength and stiffness of bio-composites in tension than in compression. As a result, the design variations are characterized by enlarged compression areas in order to reduce compression stresses, while tension zones could be kept more slender.

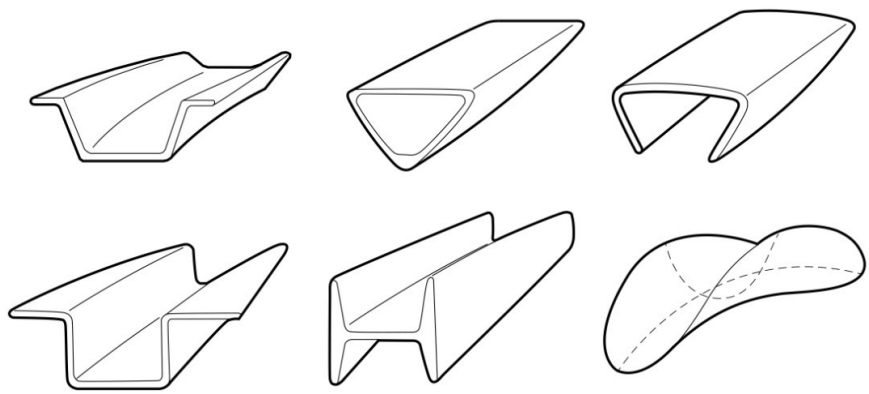

FIGURE 5.5 Workshop output on variable bridge cross-sections. R. Blok, J. Smits et al., Eindhoven University of Technology & Delft University of Technology, (2017).

The outcome of the first design phase consisted of multiple geometries as shown in figure 5.5, with various cross-sections that adopted the structural concept of either a beam, a shell or a monocoque. Solutions with U-shaped and I-shaped beams comprised solid bio-composite parapets, which increased the efficiency of the structure, while other design alternatives proposed horizontally extending top flanges, enlarging the compressive capacity of the geometry. Solutions with inverted U-shaped beams, whit enlarged compressive capacity, were considered weaker in tension and still required additional parapets on top of the structure. Also, a shell curved in two directions as shown in figure 5.5, bottom right, has been suggested as an elegant alternative solution. However, this design was not further elaborated because of the

complex and expensive mould it would have required. Finally, one of the suggested geometries had a triangular cross-section in the middle, with the point pointing down, that gradually turns into a rectangular cross section towards the abutments as shown in figure 5.5, top centre. This geometry offers high compressive strength at the level of the walking surface while still providing sufficient cross section area at the bottom for additional tensile reinforcement. Nevertheless, as this structure is in essence a monocoque shell, a vast core is required inside the NFRBP facing to act as a lost mold and to prevent collapse under vacuum production.

During the design evolution phase, the various geometries have been generated and modelled using digital parametric design tools, such as Grasshopper and Caramba, which enabled a preliminary structural evaluation of the different shape configurations, curvatures and material thicknesses in terms of maximum stresses and deflection. The sections have been evaluated on strength and section properties (second moment of inertia). The structural dimensioning of the structures were based on preliminary calculations which considered a required uniform live load of 5,0 kN/m^2 and estimated material properties.

The selection criteria that have been used to determine the geometry that was to be elaborated were: sufficient strength and stiffness, architectural appearance and cost-effective production. Besides the structural performance of the designs, aesthetical values have been equally considered throughout the design evaluation. Designs that expressed the plasticity of the new bio-composite material were favoured over more conventional solutions. As a conclusion, the solid structural parapets of the various U-beam solutions have been discarded as they would result in massive structures when seen from the side, while any attempt to create perforations in the sides would have increased production complexity and costs. Therefore, a non-structural railing solution, attached to the deck, has been justified as a more elegant and realistic solution. Weighting all parameters and evaluating the design concepts finally has resulted in the choice for the triangular monocoque deck as the design for further elaboration.

§ 5.2.2 Structural optimization of selected design

The selected deck geometry develops from a rectangular cross-section at the abutments of the bridge, into an almost triangular section of approximately 1m height in the middle of the span as shown in figure 5.6. One primary structural optimization in the direction of enhancing tensile capacity of the geometry without excessively increasing the structural height has been to turn the triangular middle cross-section

into a trapezoid with a minimum bottom width of 240mm. The bottom face increases in width towards the abutments, whilst the structural height drops and the inclined edges become perpendicular to the walking surface. This way the trapezoid cross section in the middle gradually changed into a flat rectangle at the abutments.

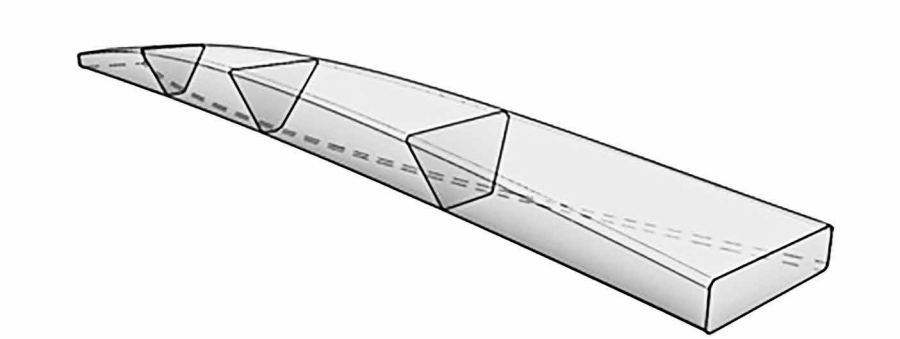

FIGURE 5.6 Different sizes and shapes of mid-span sections evaluated. R. Blok, J. Smits et al., Eindhoven University of Technology & Delft University of Technology, (2017).

Additionally, in order to further minimize deflection and increase shear capacity, the structural height at the supports of the bridge has been increased. Detailed deflection calculations have resulted in a beam height of 350mm at the abutments and a maximum beam height of 0,95m in the centre of the deck. The width of the bridge beam: the walking surface of the structure, has a constant measurement of 1,2m.

The use of NFRBP as a structural material allows for further optimization on the level of the orientation of the fibres. Thus, the bridge geometry can be further modelled and optimised using the 3D FEA software. Through the later, different material properties representing the resulting material stiffness of various combinations of fibre orientations and configurations, have been applied on areas of the bridge. Configurations with UD fibres (unidirectional), Woven fibres (two-directional) and Non-Woven fibres (random) have been compared with the aim of optimizing the deck in terms of fibre cost and structural performance. Although in design research directional fibre optimisation has been applied by using the locations and directions of the principles stresses, this has not been applied in the final design. Based on the relatively high cost of Non-Woven Uni-directional fibres the final design used woven 90 degrees flax fibres and Non-woven, randomly oriented Hemp fibres.

The areas with the lowest stresses for example the sides of the bridge-beam with low shear stresses have been designed using the low-cost Non-woven Hemp fibres. The Non-woven mats consist of randomly arranged short fibres that show consistent properties along the plane, without any dominant direction. In contrary to the woven layers that are made out of high-quality flax, the non-woven mats use the hemp fibres. The rough Hemp fibre mats have lower mechanical properties compared to flax and have been chosen to achieve a more cost-effective solution for the areas of the structure where low structural capacity is sufficient. In hindsight, when also taking into account cost of resin, this choice probably has not led to the most economical solution.

§ 5.2.3 Final materialization and detailing

The walking surface of the structure has been aligned with an upward camber with a radius of approximately 50 metre and a maximum slope angle of 6°. The deck geometry is characterized by its rounded edges that facilitate the chosen vacuum injection production technique. During a resin injection process, high pressure forces are applied evenly on the fibre mats that are wrapped around the deck. The chosen geometry from the first design phase uses a structural (hollow) bridge beam without a structural parapets, therefore and additional non-structural railing system has been designed. In order not to compromise the bio-based content of the entire structure, bio-composite has been used for the railing as well. The appearance of the railing is chosen to resemble an organic shape of grass blades, thus expressing the bio-based character of the bridge. The design consists of vertical tapered balusters that are slender at the top and widen towards the bottom where they connect with each other and to the bridge deck. For ease of fabrication, the parapets have been designed to be sawn out of sandwich laminate plates, using an open comb-like layout of the balusters allowing for two intertwined segments to be cut out of a single plate, thus minimizing cutting waste. The parapet segments have been manufactured flat, using the vacuum injection method. All segments have been bolted to the side of the deck into a timber beam that is integrated within the top corners of the core. A main characteristic of the design is the gradual outer inclination of the balusters moving away from their vertical position at the abutments of the bridge. This shifting from the vertical is a result of the evolving shape of the bridge beam itself: a gradually changing angle of the vertical sides of the bridge that is extended in the inclination of the railing. Being flexible due to its material and comb shape, the segments are able to be deformed under slightly torsional deformations that result from these changing inclinations, thus enhancing the leaf-like representation. The balusters lends a dynamic appearance to the design and bestows the feeling of an open and comfortable space to the users. To further

accentuate the leaf-like shape of the bridge, the railing has been designed with a non-constant height. The top follows an arced outline resulting in a parapet height of 1,2m in the middle of the span whilst at the abutments above the river banks the railing is only 0,9m in height.

§ 5.3 Material selection and tests for obtaining safe design values

Just like conventional fibre reinforced polymers, bio-composite is composed out of two materials; the fibres that provide the stiffness and strength are bound together by a resin, the so-called matrix that provides cohesion to the fibres and enables shear forces within the composite. Both the fibres and the resin in NFRBP can be replaced by its bio-based equivalents; natural fibres and bio-based resin. In literature [4] the approximate strengths of many different natural fibres can be found. At the start of the research project different combinations of resins and fibres that are known from literature [5] have been considered and reviewed [6]. Bamboo, hemp and flax fibres are among the fibres showing the highest failure strength. For sustainability reasons the use of locally grown fibres as hemp and flax has had our preference over bamboo. Of these two types only, the flax fibres were commercially available in directionally woven fibre mats. For this and economic reason, the flax has been applied in woven mats (90 degrees) while the cheaper hemp has been used in a non-woven (random directional) version.

With regard to the choice of resin the aim of the research has been to use a resin with a 100%, or else as high as possible, bio-based content. An epoxy-based resin has been preferred over a polyester resin because of better micro-moisture properties and also because of polyester production restrictions at the production facility. Furthermore, the number of possible resins has been reduced considerably, taken into account their commercial availability. The main important selection criteria besides availability for the remaining resins have been those properties that are most influential with regard to the vacuum injection technique. These properties are: viscosity, gel-time, hardening temperature and exothermal peak temperature. The first two properties directly influence the moulding injection plan (distances of injection to vacuum points), the latter (exothermal peak temperature) is of importance with regard of the use of the intended internal foam in relation to the maximum thickness of a single vacuum injection cycle. Some Furan based resins with a 100% bio-based content have proved unsuitable for normal production techniques because their high acid content makes them highly toxic during processing. Because of these criteria the initial goal to use a 100% bio-based resin had to be abandoned. Based on the availability of the resin as

well as the expertise of the project partner NPSP bv, Sicomin SR Greenpoxy56 with a plant based bio-content of 56% has been chosen. According to the product datasheet of the manufacturer this resin has a modulus of elasticity in tension and bending of approximately 3300 -3400 MPa and a tension breaking strength of 48 MPa.

§ 5.3.1 Initial material tests

Samples were made using the greenpoxy resin, the flax fibres, uni-directional (UD), as well as Hemp fibres (random-directional/ non-woven) to be tested.

The tension and the compression test were carried out in accordance to ISO 527 (tension) and ISO 604 (compression). The samples were 250 mm length and 25 mm width for the tension tests and 10 mm length and 20 mm width for the compression tests, 4 mm thickness. Of each fibre configuration 7 tests have been performed. Table 5.1 gives the strength results for the different resin-fibres configurations tested.

The Unidirectional fibres show higher strength values in both compression as well as tension. Table 5.2 gives expected strength and Young's modulus for the composites from a product data sheet of the supplier.

TABLE 5.1 Results per configuration and resulting values for the characteristic strength

Material	condition	Average Strength (MPa)	Standard deviation (MPa)	Characteristic (5%) Strength (MPa)
UD – Lineo	tension	202	12,6	181,3
	compression	-78,6	6,9	-67,3
UD - Scabro	tension	129,3	7,7	116,5
	compression	-104,1	4,4	-96,8
Woven Bi-direct.	tension	63,9	0,5	63
	compression	-73,5	2,1	-70
Non - woven	tension	36,1	3,4	30,5
	compression	-71,8	5,3	-63
Hybride	tension	47,5	2,9	42,8
	compression	-77,3	4,9	-69,2

TABLE 5.2 Summary of Structural Product data from N5010 Nabasco

	Tensile Strength (MPa)	Young's Modulus (MPa)
Non-woven	45	6.200
Woven, Bi-directional	69	10.500
Uni-directional	244	21.600

§ 5.3.2 Full scale production test – mock-up.

In order to test the production set-up and to establish the material properties as accurate as possible (matching the real production circumstances) a test production-run of a 2m long full-scale part of the bridge has been carried out. From this 1:1 scale element, material samples have been taken for testing. Figure 5.7 shows some milled test specimen and a test measurement set-up. Figure 5.8 shows typical test results of the composite using woven 90 degrees Flax fibres mats.

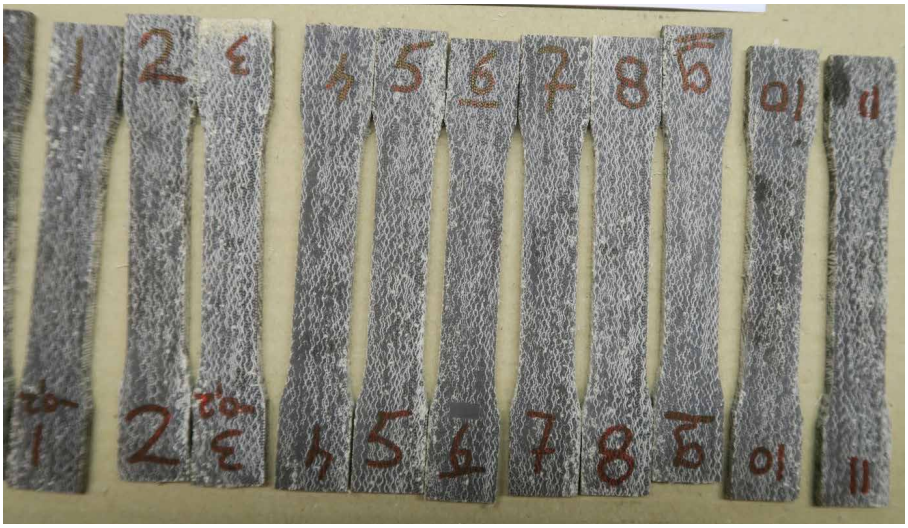

FIGURE 5.7 Milled test samples from 1:1 model and Tension test with optical strain measurement. R. Blok, J. Smits et al., Eindhoven University of Technology & Delft University of Technology, (2017).

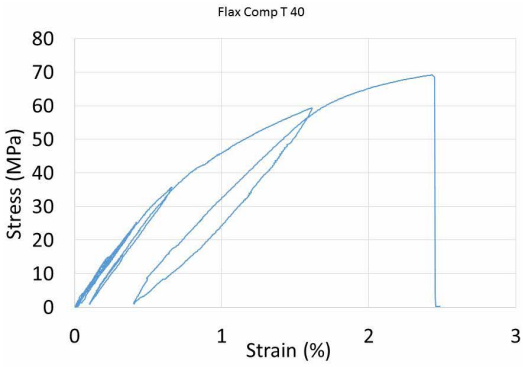

FIGURE 5.8 Typical result of a repeated loading-unloading and reloading tension test in the laboratory on a test specimen of Woven (90 degrees) flax fibre composite showing hysteresis behaviour.

From these tests, the average and characteristic strength as well as the Young's modulus has been calculated to be used in the final structural calculation. The characteristic 5% limit value of the material strength of these samples' (No's: 33) was 60 MPa. Calculating the Young's modulus from these data in the stress range of use resulted in an expected E_{avg} = 7.500 to 10.000 MPa. The Young's modulus value of 21.600 MPA provided by the supplier was thus found to be considerably higher than the value found in our own tests. To arrive at safe design strength values from experimental test data a similar approach as used in the Dutch recommendation design code for GFRP: CUR 96 has been followed. Based on this approach, the characteristic strength has been reduced by a material factor γ_m, representing mainly the estimated production influences as well as a conversion factor γ_c, representing estimated influences of long-term material behaviour due to temperature, moisture, fatigue and creep influences. This approach resulted in a applied design strength of roughly 25 % of the characteristic value. The material factor γ_m has been conservatively estimated as 1,89 while the conversion factor γ_c has been estimated as 2. The resulting design value Rd = Rk/ (γm * γc) was thus calculated as 15,9 MPa.

§ 5.3.3 Moisture tests

To estimate the influence of moisture, samples submersed in water have been tested, both at Delft University of Technology as at Eindhoven University of Technology. Tests have been performed in accordance to ASTM D 5229/5229M-14. The test in Delft were conducted using a weathering facility that mimics accelerated cycles of moisture/

draught, high/low temperatures and UV light cycles. These tests are not discussed here but have shown similar results to the test performed at Eindhoven. In these later tests, samples have been submersed in water and then tested after different periods of submersion. Oven dry samples have been compared to samples with other moisture content. The thus obtained values did not show a decrease in tensile strength for the submerging in water for 24, 48 and 96 hours compared to oven dried specimen (with a moisture content of 7,5 %). The measured strains however showed a large increase with longer submersion and higher water content compared to dry samples. The quality of these test and its results is questioned however, because test samples had been sawn out of a larger plate, leaving the end of its fibres exposed to direct water contact. No final conclusions have been drawn other than that strains clearly increase with increased (fibre-) water content and therefore protection measures of the composite material and in particular its fibres against outside water clearly was needed.

§ 5.3.4 Creep tests

Because it was expected that the bridge will also show time dependent non-linear behaviour, creep test have been performed (figure 5.9). Three-point bending material creep tests on three different stress levels (5 MPa, 15 MPa and 25 MPa) have been performed at TU/e. Figure 8 shows the results of these tests.

FIGURE 5.9 Creep test set-up at TU/e laboratory. R. Blok, J. Smits et al., Eindhoven University of Technology & Delft University of Technology, (2017).

The creep slope of the samples under lower stress levels (indicated with 5 MPa) hardly show a decrease in time. The higher stress level (25 MPa) shows only a very small reduction in the creep slope. Therefore, the long term deflection of the bridge can be estimated by a reduction in E-modulus approach, using with a reduction factor k_{def}:

$E_{mean,fin} = E\ mean / (1 + k_{def})$.

Based on the creep curves for the low stress-levels of 5MPa (figure 5.10) and preliminary calculations, a k_{def} = 0,8 was found and applied in the design calculations

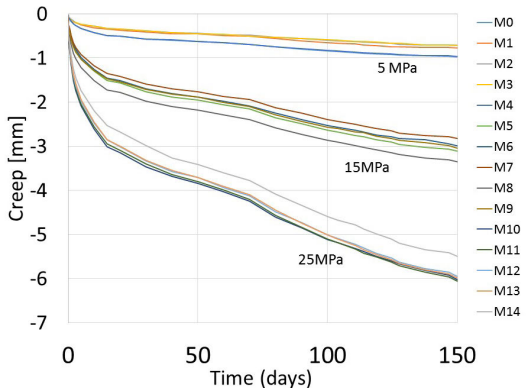

FIGURE 5.10 Creep curves at three stress levels 5, 15 and 25 MPa in three-point bending tests.

In order to avoid large creep deformations in the bridge design, the stress levels due to the permanent load (bridge beam and balustrade) needed to be kept low, preferably lower than the value of 5 MPa as used in the creep tests.

§ 5.3.5 Monitoring strains using optical sensors

Given the still remaining uncertainties of long-term material behaviour, as well as the opportunity to obtain more data during Service Life of the bridge, it has been decided to monitor the bridge on site by integrating sensors in the bridge structure. The monitoring is carried out by Eindhoven University of Technology, on whose campus the bridge lies. Optical Fibre Bragg Grating sensor technology (FBG) has been used because of its non-intrusive nature, its small dimensions as well as its high sensitivity

[7]. Constantly monitoring the bridge behaviour remains a goal for the future but for economic reasons (with regard to the necessary equipment for constant monitoring), a number of separate tests have been performed instead. The thin glass fibre based sensor lines (~100 – 200 µm diameter) that were used are extremely vulnerable during production. For this reason, the glass fibre has been glued between two layers of Uni-Directional (UD) fibres for protection. Figure 5.11 shows the preparation of these glass fibre sensors, UV-glueing the sensors between two layers of Uni-directional Flax fibres, before integrating the protected sensors in the production process.

FIGURE 5.11 Preparation of optical (glass) Fibre Brag Grating sensors. R. Blok, J. Smits et al., Eindhoven University of Technology & Delft University of Technology, (2017).

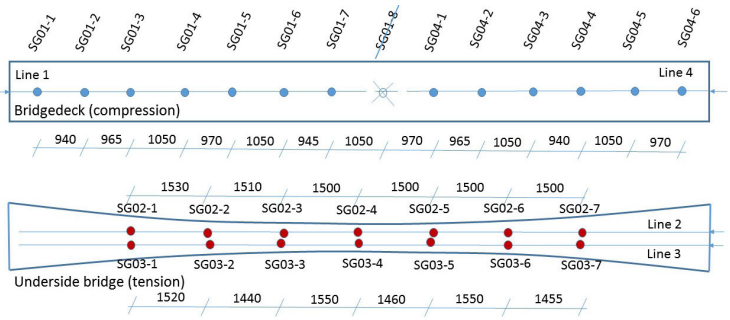

FIGURE 5.12 Location of Sensors. Line SG-01 and SG-04 are mainly compression (in bridge deck). Line SG-02 and SG-03 are mainly tension (under-side bridge). R. Blok, J. Smits et al., Eindhoven University of Technology & Delft University of Technology, (2017).

A total of 28 sensors have been installed in initially 3 lines. Figure 5.12 shows the location of the 28 integrated sensors in a schematic top –and bottom view of the bridge.

Unfortunately, the compression line broke during production, for which reason only the sensors SG01-1 to 01-7 on the compression side were registered during the test of October. In the test of December 2016, the sensors SG 04-1 to 04-6 could be recovered by accessing them from the other side (line 04). Sensor 01-8 was lost

§ 5.4 Production process

The basis for the production of the bio-composite footbridge is a proven vacuum injection method with a lost mould system. In brief, the building process starts with the shaping of the internal core of the structure in bio-foam acting as a lost mould. Next a series of various bio-fibre mats are applied to all sides of the lost mould. The fibres are then wrapped in a vacuum bag with a network of injection and vacuum canals connecting to a vacuum machine on the one side and barrels of bio-resin connected to the vacuum bag on the other side. The vacuum results in the resin being sucked into the fibres where the hardening process of the resin (resin mixed with hardener) takes place.

The decision for a lost foam mould was taken to prevent the use of an external (costly) mould. PLA foam was chosen as a bio-based solution. PLA, also known as polylactide, is an aliphatic thermoplastic polyester produced from renewable resources that is compostable when exposed in the environment. The PLA foam core was made out of transversal laser cuts layers that gradually change the shape of the bridge over its length, from a rectangular shape at its ends, towards a triangular shape in the middle section. Figure 5.13 shows this approach for one half of the bridge design.

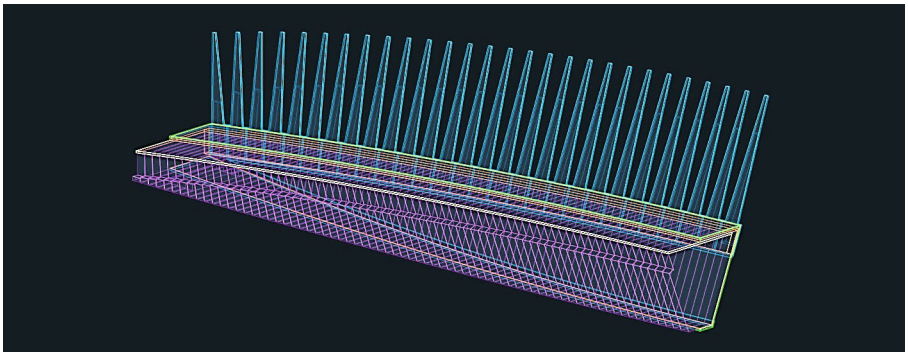

FIGURE 5.13 Change in shape from rectangular to triangular using laser cut PLA foam elements. R. Blok, J. Smits et al., Eindhoven University of Technology & Delft University of Technology, (2017).

This forming approach thus avoids an expensive mould-systems and it has been combined by producing the bridge top-side down on a curved ramp. This produces the slightly curved shape of the walking surface of the bridge. PLA has a low melting temperature of about 80 Celsius, while the exothermal peak of the used bio-resins while curing can become 135 Celsius or more. The temperature peak during curing depends on the thickness of the NFRBP layer. Figure 5.14 shows how the heat generated from curing increases with the thickness of the lay-up and causes melting of the PLA. It was therefore decided to prevent excessive heating and melting of the core limiting the maximum production thickness of the composite in contact with the PLA to 10 mm as well as d by avoiding direct contact between the bio-resin and the PLA through the use of a layer of insulated cork material between the PLA and the NFRBP. Additionally, water cooling was used to further prevent the internal PLA core structure from melting down.

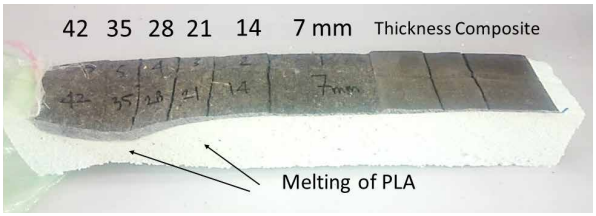

FIGURE 5.14 Meltdown of the PLA foam occurred when the thickness of the lay-up exceeds 10mm. R. Blok, J. Smits et al., Eindhoven University of Technology & Delft University of Technology, (2017).

Additionally, a prefabricated layer, a laminate of structural NFRBP was introduced to arrive at the structural required thickness of 20 mm in top and bottom flange of the bridge beam. This prefabricated laminate layer of 10 mm was added in both top and bottom of the bridge beam before the final injection, see figure 5.15, thus minimising the exothermic heating load on the PLA.

The final built-up of the structure is as follows: the PLA foam inner core is covered by a thin layer of cork material, on top of that the woven Flax (linen) is applied on bottom and top corners as well as the prefabricated (and perforated) laminates on top and bottom which itself is again covered with fibres. In the less loaded parts (the side flanges of the bridge beam) the non-woven flax and hemp mats are used. Figure 13 shows the position of the 90 degrees woven fabric, indicated in red. The whole bridge beam element has been vacuum injected with the bio-based epoxy resin Greenpoxy 56 (77,5% Greenpoxy 56 resin, 22,5% 4770 hardener). The hardening occurs effectively under the vacuum compression resulting in a high fibre to resin ratio and higher composite strength.

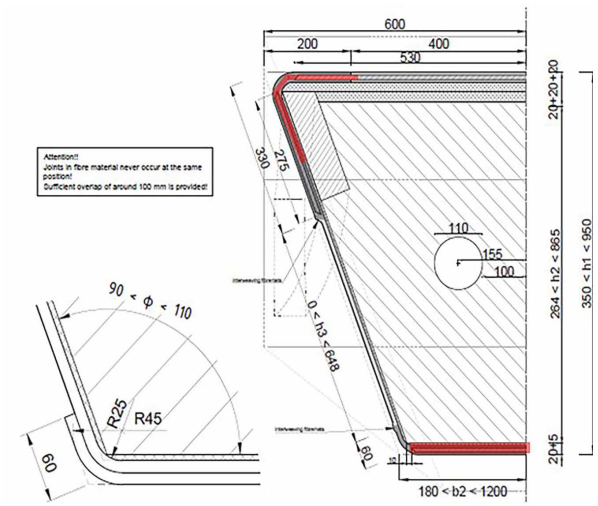

FIGURE 5.15 Part of a Production drawing, (half of section in middle of the bridge, in red/dark is indicated the position the woven fibres. R. Blok, J. Smits et al., Eindhoven University of Technology & Delft University of Technology, (2017).

FIGURE 5.16 Bridge beam during Vacuum injection. R. Blok, J. Smits et al., Eindhoven University of Technology & Delft University of Technology, (2017).

Figure 5.16 shows the injection of the bridge beam (in top down position). In the dark green coloured areas, between the yellow injection canals, the resin has already penetrated the fibres. After the vacuum injection and the hardening, the bridge beam was turned 180 degrees and then cured at a temperature of approximate 50 Celsius for a 36-hour period using electrical air heaters. The bridge rail elements were then mounted and lastly, to prevent moisture accessing the structure over time, a coating system was applied.

§ 5.5 Structural behaviour of the bridge

§ 5.5.1 Load test after production, installation

Before the installation on site, the bridge has been tested as part of the construction permit application process on October 16th at the production facility. During a calibration test with water tanks the live load was gradually increased from 0 kg/m² up to 475 kg/m², in line with the standard requirement for footbridges (5,0 kN/m² minus a 5% reduction based on the length of the bridge). Figure 5.17 gives an impression of the load-test set up. The load has been applied evenly by filling 7 cubical tanks with water. During the test, the deformations of the bridge was measured using LVDT's (vertical and horizontal displacements) at 6 different points. At the same time the strains in the optical sensors were measured and compared to an elastic beam model as well as a FEA model.

FIGURE 5.17 Impression of the load test using 7 water tanks.R. Blok, J. Smits et al., Eindhoven University of Technology & Delft University of Technology, (2017).

Figure 5.18 gives the calculated end-values of the vertical deflections, the longitudinal compression and tension stresses and the strains based on a linear elastic model with a Young's modulus of 10.000 MPa in the load test under the maximum load.

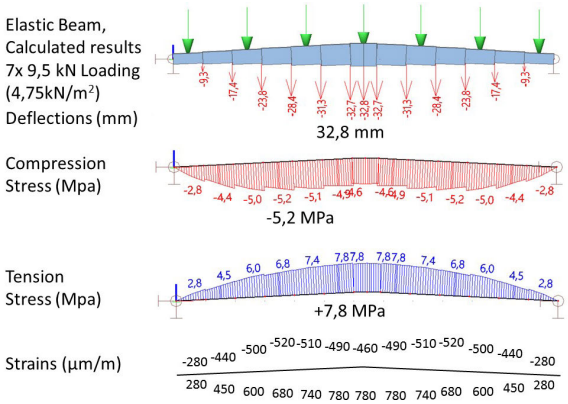

FIGURE 5.18 Elastic Model, calculated vertical deflections, the longitudinal compression and tension stresses and the strains.

The results of the measured LVDT deflections with water tanks filled in steps of approximately 100kg/m² can be seen in figure 5.17, The calculated value of 32,8 mm in the elastic model almost exactly matches the measured value: 33,1 mm. The measured strains in the optical sensors equally showed a very good correlation with calculated strains. The maximum measured strain on the tension side was about 800 μm/m compared to

780 µm/m calculated. On the compression side, the measured strain was about 550 µm/m compared to 520 µm/m calculated, this is within a 2,5% to 6% difference.

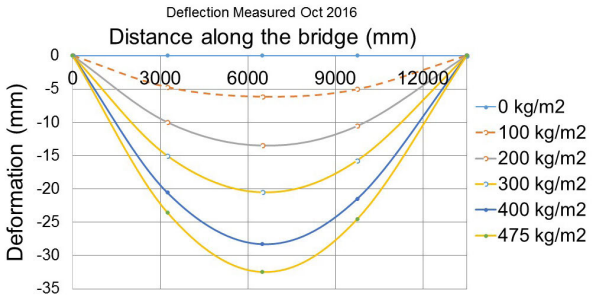

FIGURE 5.19 Results measured LDVT Deflections at Production facility test October 21th 2016.

In figure 5.20 the measured strain deformations are given as function of the applied load over the length of the bridge, again in steps of about 100 kg/m^2. The linear behaviour of the bridge for each sensing point is shown. A relationship between deformation and deflection could be derived and used during the field test to extract the deflection of the bridge during in-situ loading.

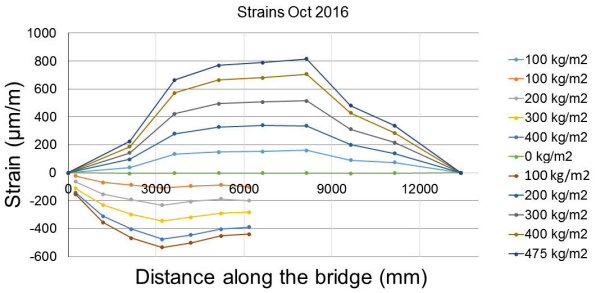

FIGURE 5.20 Strain deformations as function of the applied load.

Figure 5.21 shows the strain development of the same test but now with the strains in the indicated different sensors in relation to the time of an almost two-hour period, while filling the water tanks. The small horizontal parts are a pause in the filling of the water tanks.

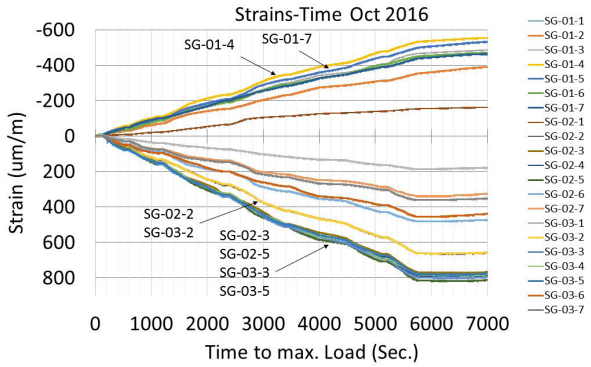

FIGURE 5.21 Strain development versus time during loading; Lines 2 and 3 are positive strains in tension (underside bridge-beam) line 1 shows negative strains in compression (in bridge deck).

The preliminary conclusions from the production facility test were that the bridge's initial (non-long term) behaviour closely follows the expected behaviour of the design models and that the bridge was able to successfully carry its full maximum design load.

§ 5.5.2 In situ measurements in use phase

After preliminary installation in November 2016 the bridge's bearings were slightly raised to prevent the curved bridge beam touching the retaining wall. For this reason, the test performed at 15-12-2016 after the adjustment of the bearings was taken as the initial Zero Measurement. The strains were measured without applying additional loads.

§ 5.5.3 Dynamic test 15-03 2017

On 15-03-2017 a static load test was performed but also a simple dynamic test was carried out. This was done through a simple heel test in the middle of the bridge. A person, standing on his toes and dropping flat to his feet, generated a vertical impulse load. Figure 5.22 shows the measured strains that were invoked in this way versus the time of sensors SG-01-1-7 and SG 01-2-4, both in the middle but at opposite sides, top and bottom, of the bridge.

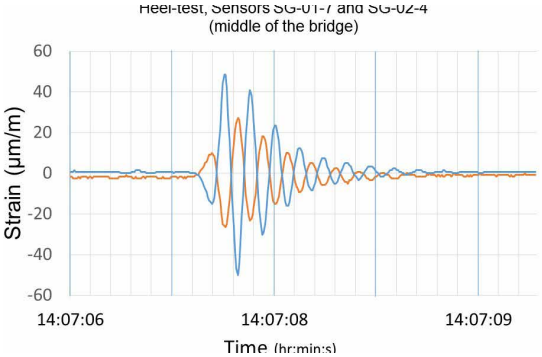

FIGURE 5.22 Strain results versus time of Sensors 1-7 and 2-4 showing eigenfrequency and damping.

Based on these measurements the Eigen frequency of the bridge the first (vertical) vibration mode has been calculated at 6 Hz (lying out of the zone of 2.5 Hz < f_n < 4,6 Hz where discomfort due to larger accelerations might occur). Also the logarithmic decrement δ = 0.58 in a free decay of the vibration and the damping factor ζ =0.093 was calculated using $\delta = \frac{1}{n} ln(\frac{x_0}{x_n})$ and $\zeta = \frac{\delta}{2\pi}$ in which ζ = damping factor, δ = logarithmic decrement, n = number of cycles, x_0' = amplitude of the 1st cycle, x_n = amplitude of the nth cycle. This relatively high damping compared to for example steel or concrete bridges further contributes to a good dynamic behaviour and pedestrian comfort.

§ 5.5.4 Static Test 17-08-2018

The latest test thus far has been the test performed on August 17th, 2018, 22 months after the installation. In this test two water containers have been used to impose a load of a maximum of 2x 10 kN in a cyclic loading test (figure 5.23). Each load cycle step involved loading by filling the water tanks and unloading by releasing the water. The first load cycle has been performed in 3 steps to 2x 6,0 kN. After each load step of 2,0 kN a five minute break was implemented during which time the load was kept constant in order to see if an increase in strains was measured. Figure 22 shows the full 3 loading and unloading cycles versus time. Load cycle 2 was the reloading to 2x 10 kN and the full unloading and cycle 3 was the reloading once more to 10 kN and unloading to 0 kN.

FIGURE 5.23 Cyclic loading test performed one year and ten months after installation. R. Blok, J. Smits et al., Eindhoven University of Technology & Delft University of Technology, (2017).

The strains have been measured using the integrated FBG sensors. On the tension side of the bridge the results have been successfully measured. The measurements in the compression side however showed unreliable results. It is expected that the reason for this is that the sensors were not embedded in woven flax material but in unwoven less structural functioning Hemp material (in the middle of the bridge deck). Therefore, the contact of the glass fibres with its sensors to the non-woven, randomly oriented hemp fibres was unstable. For this reason only the tension side results are shown here. During the test, vertical deflection of the bridge was also measured (middle of the bridge) using an optical device (see also figure 5.24 in the middle).

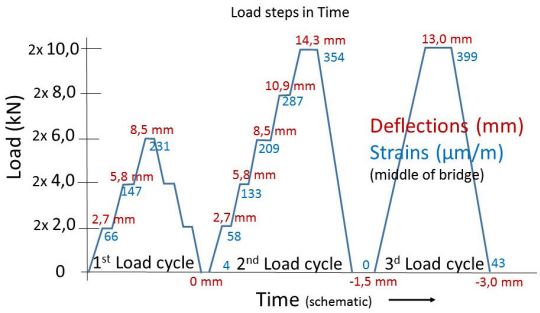

FIGURE 5.24 Three load cycles during the test on 17-08-2018 showing applied load, max strain in middle and maximum measured vertical deflection.

The strain results for the tension line 02 in the first load-cycle to approximately 600 mm water per tank (6,0 kN) and back to zero are shown in figure 5.25. The results of the second cycle are shown in figure 5.26.

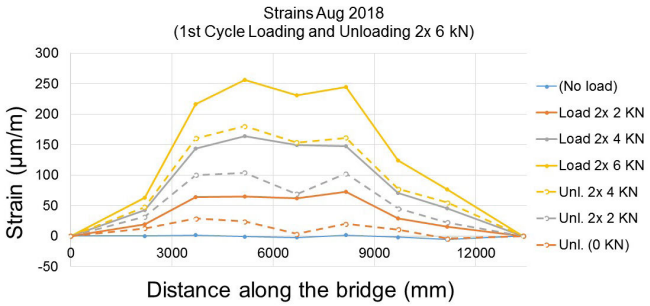

FIGURE 5.25 First Load Cycle; Results of strains in tension sensors along the bridge (Line 2), Loading and unloading to 2x 6,0 kN.

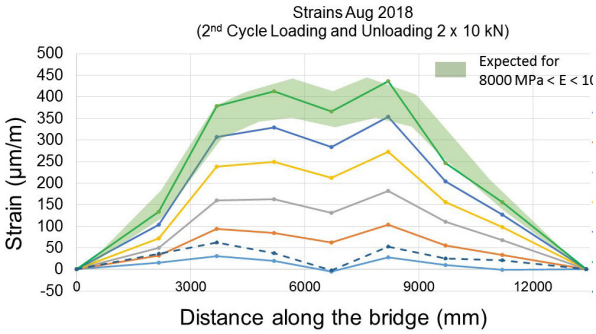

FIGURE 5.26 Second Load Cycle; Results of strains in tension sensors along the bridge (Line 2), Stepwise Loading and unloading to 2x 10,0 kN.

The green bandwidth shows the expected values of the strains calculated using an elastic calculation with a Youngs modulus between 8.000 and 10.000 MPa. While the strains in the middle of the bridge return to 0 there are small remaining strains on the left and right site of the bridge. The dotted line shows these remaining strains. This effect is increased after the third load cycle. Figure 5.27 shows the results of this third load cycle.

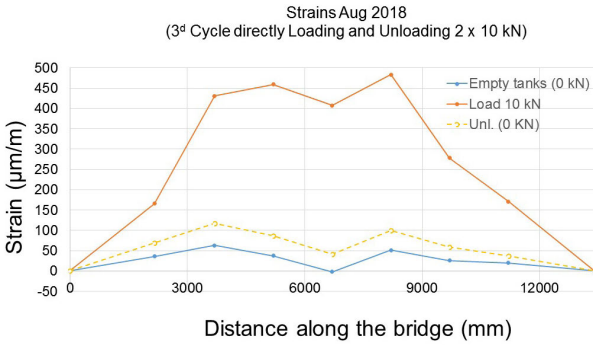

FIGURE 5.27 Third Load Cycle; Results of strains in tension sensors along the bridge (Line 2), Loading and unloading directly to 2x 10,0 k. The dotted line shows the remaining strains.

The second loading to the full 2x 10 kN load show almost 50 µm/m higher maximum strains near the middle of the bridge. Also, the unloading shows remaining overall strains of approximately 50 µm/m near the middle of the bridge. The sensors indicate a process of "yielding", the increasing deformation under the constant load, not fully returning to the starting position of the sensors. The visual deflection measurements however do not show this yielding effect. Figure 5.28 shows the measured deflection in the middle of the bridge. The bridge shows a lasting upward deflection of initially almost 2 mm and at the third cycle an upward deformation of about 3 mm. A cause for this could be sought in small horizontal reactions at the (rubber) bearings of the bridge in loading. Because horizontal movement here is not fully free due some friction, some very small compression arch-like action is possible. Also, during unloading of the bridge there might be some remaining horizontal inward reactions, resulting into small upward bending moments at the bearings. Since the horizontal deformations have not been measured other explanations such as temperature deformation might also be a cause for this phenomenon. The measurements started in the morning and during the testing period the sun gradually warmed the top of the bridge deck. Modelling a temperature difference of 10K between bridge deck and underside in an elastic beam model results also in a 2,8 mm upward deformation in the middle of the bridge. It can therefore be assumed that the influence of the sun may have influenced the variations found in strains and deflections.

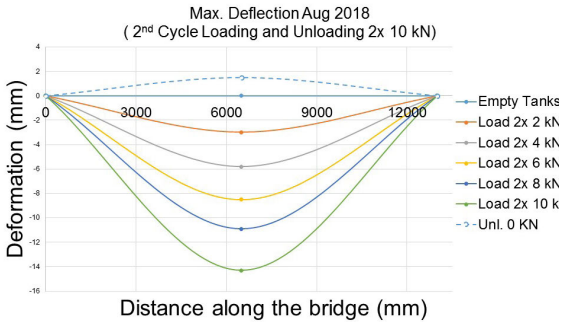

FIGURE 5.28 Measured deflections (in middle of the bridge) during second loading (10 kN) and unloading cycle.

The elastic response to short time loads seems to show a more or less constant or only slightly decreasing material stiffness of approximately 10.000 MPa similar to the elastic beam model. The strains show a good correlation when the additional "yielding" strain is ignored. The calculated maximum strains in tension of 350 µm/m is also measured using the FBG's. Also the maximum strain of about 450 µm/m minus the remaining strains after unloading, 85 and 100 µm/m show a difference of about 365 to 380 µm/m comparable to the calculated value of 350 µm/m. (Maximum reduced modulus of elasticity can be calculated as (350/380) x 10.000 MPa = 9200 MPa) Also the measured deflections of about 16 mm (figure 26) compared to the calculated deflection of 14,6 mm (figure 5.29) support this slight reduction in stiffness.

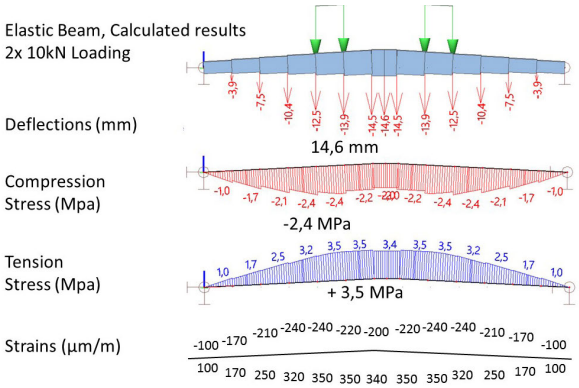

FIGURE 5.29 Elastic Model, calculated vertical deflections, the longitudinal compression and tension stresses and the strains based on Young's modulus 10.000 MPa under maximum of 2x 10 kN: maximum deflection = 14,6 mm.

§ 5.5.5 Long term behaviour

Differencing from the short time more or less elastic loading behaviour however, it could already be expected, from increasing strains under a constant load in the initial load tests and the strains not fully returning to 0 after unloading, as well as from the performed creep tests that the bridge itself would also show creep behaviour. The measurements conform this creep behaviour. Figure 5.30 shows the strain measurement results of the middle sensor (SG02-4) over a 20,6-month period. It compares the strains of the different tests in time. The strains show a considerable increase in time, indicating that the bridge shows considerable creep deformation. It appears that the creep process has not yet come to an end, despite the relative low stress levels of the long-lasting self-weight of the structure (maximum 2,1MPa in compression and 3,3 MPa in tension). The dotted line shows an expected behaviour however further tests are needed to confirm this.

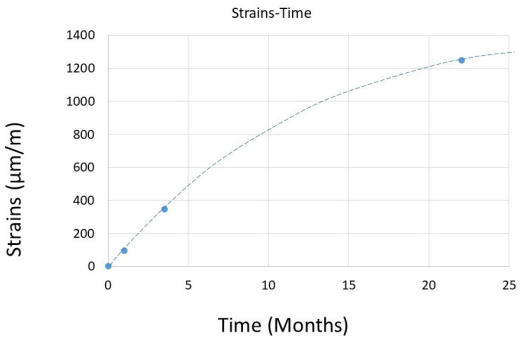

FIGURE 5.30 Strain measurement results of unloaded bridge (only self-weight) of 5 measurements in time.

Calculated from these strains the deformation in the middle of the bridge is now estimated at 51 mm. In the design stage the creep deformation (based on a calculated $E_{mean,fin} = E\ mean/(1 + k_{def})$ with a $k_{def} = 0,8$ was estimated at approximately 15 mm. The measured and calculated creep therefore is much larger than expected from the initial creep test results and also this creep deformation has most likely not reached its final value. For future use of NFRBP as a load bearing material for footbridges, a longer Service Life needs to be achieved. Therefore, the creep deformation needs to be further limited and kept within bounds.

§ 5.6 Life Cycle Assessment

To achieve complete insight over the environmental impact of the bridge, a literature-based LCA [8–13] focusing on the material production phase, the use phase and the end of life scenario, has been performed. The assessment has been based on the environmental impact over eight impact categories listed in ISO/TR 14047:2003: abiotic depletion potential (ADP), global warming potential (GWP100), ozone depletion potential (ODP), photochemical oxidant creation potential (POCP), acidification potential (AP), eutrophication potential (EP), human toxicity potential (HTP), freshwater aquatic ecotoxicity potential (FAETP), marine aquatic ecotoxicity potential (MAETP), and terrestrial ecotoxicity potential (TETP).

To achieve a clear comparison between the environmental costs of the different materials of the bridge, the LCA data shown in Table 4 have been translated into environmental cost impact (ECI) values, shown at the bottom the table. The ECI values, measured in Euros, balance the environmental impact categories by using shadow cost factors [14] which allow for adding the impact categories into one value.

§ 5.6.1 Production

The first step has been to determine the impact of the main raw constituent materials of the bridge individually in terms of their production. The materials that have been considered in this part of the analysis were the flax fibres, the hemp fibres, the bio-based epoxy resin, the PLA foam core, the cork layer, the coating and the anti-slip layer. Calculating the material quantities used for constructing the bridge (table 5.3) and linking them with the LCA data (table 5.4), has revealed the actual degree of environmental impact for the total of materials used to build the bridge (figure 29).

TABLE 5.3 quantities of materials used to construct the bridge

Material	Flax 2x2 twill (400g/m2)	Hemp non-woven mat (380g/m^2)	Bio-based epoxy	PLA (35 kg/m3)	Paint (125g/m^2)	Antislip layer (4,5kg/m^2)
Weight [kg]	136.53	84.10	661.89	247.10	11.65	75,69

Production of flax and hemp fibre is a result of a series of agricultural and fibre-processing operations. A typical production cycle consists of several stages, beginning with soil preparation and planting of the seed until harvesting, which is followed by processes such as retting, hackling and spinning. A number of these stages can be employed though by a wide range of different techniques which may vary in terms of energy demand. Once the fibres are spun into yarns, then technical textiles, mats and apparel fabrics are being produced by being either woven, knitted or processed through other techniques. Environmentally weak points of the production of flax and hemp fibre are mainly linked with the extensive use of chemical fertilizers and pesticides based on nitrogen, phosphorus and potassium. High nitrate and phosphate emissions contribute to increased eutrophication in local water-bodies and soil as these elements become main nutrients for algae growth. Subsequently, major deterioration of water quality results in the loss of aquatic life and hence disruption of the ecosystem.

TABLE 5.4 LCA per kg of the main constituent materials of the bridge8- 13

Impact category	Units	Hackled flax, 1kg (Duigou, Davies, & Baley, 2011)	Hemp mat, 1kg (Rosa et al., 2013)	Bio-based epoxy SuperSap, 1 ton (Rosa et al., 2013)	Corn based PLA 1kg (Environ-mental factsheet: Polylactic acid, 2016)	Spray painting, 1 kg (MRPI, 2013)	Petroleum based epoxy resin, 1 ton (Rosa et al., 2013)	stone chippings, 1 kg (Benelux Bitume & VBWAsfalt, 2005)
ADP	Ab eq.	1.70E-03	4.00E-03	0.01	-	0.03	59.4	1.50E-04
GWP100	CO_2 eq.	-14	0.531	4079	0.6-3.2	2.4	6663	2.10E-05
ODP	CFC-11 eq.	2.40E-08	6.88E-08	0	4.0E-10 -3.6E-07	1.40E-07	1.26E-06	5.10E-05
POCP	C_2H_4 eq.	7.30E-05	-	-	6E-04 -1E-03	0.12	-	0.02
AP	SO_2 eq.	2.20E-03	2.60E-03	25.44	7.3E-03 -3.8E-02	0.014	40.3	3.30E-03
EP	PO_4 eq.	1.40E-03	6.00E-04	6.9	1.8E-04 -7.5E-03	1.60E-03	6.6	2.50E-04
HTP	1.4-DCB eq.	0.215	0.136	545.17	7.50E-08	5.7	490.44	3.00E-03
FAETP	1.4-DCB eq.	0.059	0.0571	66.39	-	0.83	246.5	7.80E-04
MAETP	1.4-DCB eq.	-	131	-	0.03	45	-	-
TETP	1.4-DCB eq.	8.70E-03	1.52E-03	228.63	-	0.036	29.1	3.10E-05
ECI	€	0.0265	0.0701	0.4326	0.1597	0.9798	0.6070	0.0633

The use of mechanical agricultural operations and fibre extraction processes increase the energy consumption while extensive land use of agricultural productions is another factor that adds on the environmental impact of the fibre. Table 4 shows the environmental impact of hackled flax fibres that have been cultivated and processed in France. The negative sign of the total value is due to the negative Global Warming Potential (CO_2), which is a result of the consumption of CO_2 by plant fibres.

Regarding the bio-based resin, SR Greenpoxy56 has been used in combination with the non-bio-based hardener SD 4770 produced by the same company. Although up to 56% of the molecular structure of Greenpoxy has been derived from plants, the combined product, due to the hardener, drops to a total bio-based content of 43%. The unavailability of LCA data on Greenpoxy56 which has been used in the bridge has directed the research into data from a similar bio-based resin available in the market. Therefore, the bio-based epoxy SuperSap, which has a 37% bio-based content and is produced by Entropy resins, has been used as an alternative in the present analysis as LCA data on SuperSap are available.

The LCA has revealed that the epoxy resin is the highest total contributor in the total environmental cost of the bridge, while the painting has the highest relative costs per kg. According to Rosa et al. [9] global warming potential presents the highest values while acidification potential and human toxicity follow with significant environmental impact, compared to the other materials.

PLA foam, contrary to fossil fuel-based foams, consists of natural raw resources. The main two constituent products that synthesize polylactic acid are sugars, such as glucose or lactose, and Lactic acid which is produced by the fermentation of sugars based on biomass (starch, sugarcane, corn). The environmental impact data that has been used in table 4 concerns foam based on corn.

Concerning the protection of the composite laminate from moisture, UV light and other harmful environmental factors, the application of a layer of coating has been essential. Paint typically consists out of solvent, pigment, resin (binder) and additives. Negative environmental impact of paint is mostly linked with the emission of volatile organic compounds (VOCs) during the drying phase, causing excessive formation of ozone, a highly toxic component which increases human health risks. To reduce these harmful emissions, less-VOC or no-VOC products are currently becoming available in the market.

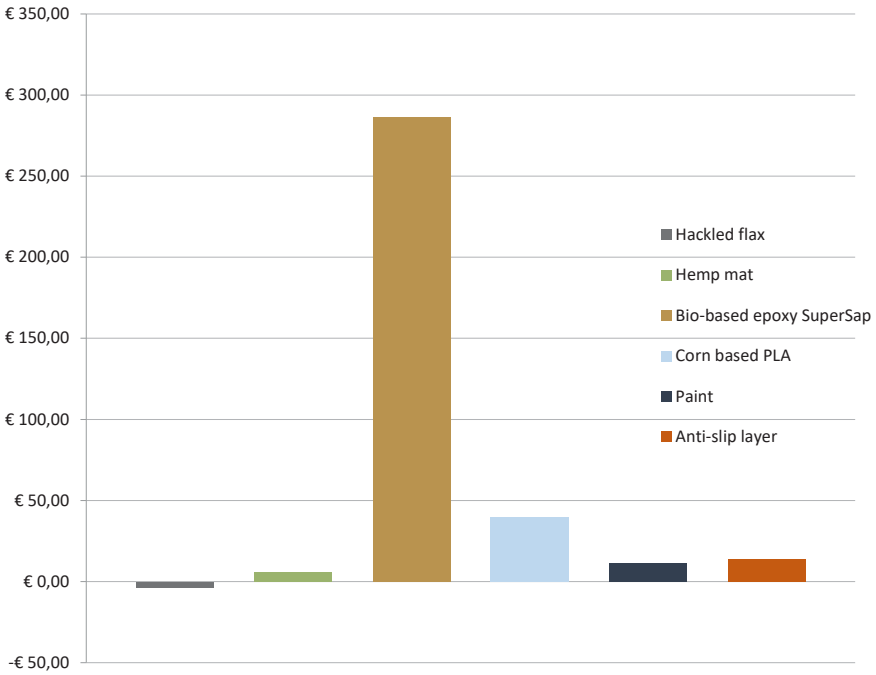

FIGURE 5.31 Environmental cost impact for the total material used in to build the bridge.

The anti-slip layer that has been applied for safety on top of the walking surface is composed out of a two-component epoxy system combined with grains (Mandurax). The LCA data that has been used for the grains refers to stone chippings, which are used in road construction for providing roughness to the asphalt [12]. The composition of the chippings has been based on a combination of different types of stones such as gravel and granite. The data includes transportation of the quarried raw material from the mining area, crushing into finer particles, washing and transportation to the asphalt manufacturer.

§ 5.6.2 Use phase

The environmental impact of the use phase of the structure focuses on the maintenance of the bridge during a service life of 50 years. Maintenance of the coating has been estimated to occur every 12,5 years for local surface deterioration areas while it has been suggested that the coating is to be totally renewed every 25 years (BECO 2013). The contribution of coating maintenance to the environmental impact of the bridge during its service life is € 11,42

Similarly, the anti-slip layer has been assumed to be renewed once during the 50-year life time. During that process, a new layer of grains mixed with an epoxy resin will have to be applied on the original walking surface after it is cleaned from remaining parts of the first layer. The addition of the new layer will add an environmental cost of € 13,94.

§ 5.6.3 End of life scenario

As bio-based composites are relatively new materials in the building industry, alternative end-of-life scenarios are still at the level of research. The most common assumption is that energy will have to be recovered by incinerating waste bio-composites. Nevertheless, the material offers recycling potentials that are currently under development.

A chemical recycling method that aims to detach and reuse the resin and the fibres is currently under examination by the Center of Expertise Biobased Economy in the Netherlands. The method performs solvolysis reactions on carbon fibre-reinforced composites which results in the separation of the two components [13]. The subtracted materials offer possibilities for down-cycling as they lose part of their initial properties during the chemical process.

Considering the experimental character of the bio-based composite bridge, a convenient and productive way to end its service life could be the continuation of further research through actual testing until failure on the bridge. The segmentation of the structure in units and the examination of these by different institutions could bring fruitful results in regard to reuse and recycling solutions of fibre-reinforced polymer structures.

§ 5.7 Conclusion

The starting goal of the project, namely to design and build a bio-composite bridge structure with a maximum bio-based content and monitor its behaviour in the use phase has proven to be successfully achieved. The conducted research on the NFRBP footbridge has enlarged the overall knowledge and experience with the design, production and use of a NFRBP footbridge structure.

The use of Fibre Brag sensor techniques in the bridge proved to be largely successful. The sensors applied in the Woven Flax material on the tension side are still operating reliable without problems. The sensors applied in Non-Woven Hemp fibre composite (the compression side of the bridge) were less successful. After the initial measurements these sensors gave unreliable results and at the last measurement session the connection did not work. In hindsight it would have been advisable to use also on the compression side two senor lines and to incorporate these lines in the woven Flax fibre composite materials instead of in the less structural middle part of the deck (with Non-woven hemp fibres). The strain measurement results of the bridge in use proved to be consistent with the measured material behaviour in laboratory tests. The long-term creep behaviour measured in the bridge proved to be larger than expected from laboratory creep tests. For future Bio-composite bridges the material behaviour in creep needs be improved.

The LCA of the finalized footbridge proved a useful tool to determine the overall environmental impact of the bridge. It also demonstrated that there is still room for improvement on the material side of bio-composites. The LCA has proven that the one ingredient of the bridge that is responsible for the vast majority of the total environmental impact is the (semi-) bio-resin. Part of this finding can be explained by the absence of LCA data for the SR Greenpoxy56 resin that was used. The bio-resin that was used instead to determine the environmental impact has a bio-content of 37%, whereas the Greenpoxy that we used has a 56% bio-content. It is also notable that the non-biological hardeners that were used for the curing constitute a substantial volume amount of the combined product, making its bio-content drop from 56% to 43%. It is therefore necessary to conduct further research into bio-resins as well as bio-hardeners to further decrease the environmental impact of NFRBP structures.

Acknowledgments

This Bio-based composite footbridge project research has been made possible under a so called 3TUlighthouse project funding. The project team members were: Eindhoven University of Technology (Project-leader), Delft University of Technology, the company NPSP BV, and the Centre of Expertise Bio-Based Economy, Breda, Netherlands. Because of close cooperation with the Bio-based bridge research project, financed through the Dutch Stichting Innovatie Alliantie (SIA RAAK) additional funding for the fabrication of a full footbridge became possible and results from this project could be incorporated. And last but not least, the Bio-based composite footbridge could not have been built without and the help of many students.

References

[1] Geldermans, B., Luscuere, P., Jansen, S., Tenpierik, M. (2016). Beyond Cities: Materialen, producten & circulair bouwen. *TVVL Magazine*. 45(1): 22-25.

[2] UNFCC Paris Climate agreement (2015). *Adoption of the Paris agreement*.

[3] NOW Dutch national research agenda (2016). *Theme Energy and raw materials: Circular economy.*

[4] Andersons, J. (2011). *Tensile strength model of UD flax fiber reinforced polymer composites*. 4th International Conference on Experiments/Process/System Modeling/Simulation/Optimization 4th IC-EpsMsO Athens, Greece, Volume: Vol. 2, pp. 620-625

[5] Al-Bahadly, E. (2013). *The mechanical properties of natural fibre composites*. Faculty of Engineering Swinburne University of Technology. Doctoral Dissertation.

[6] Zini, E., Scandola, M. (2011). Green composites: an overview. *Polym Composite;32*(12):1905–15. doi:10.1002/pc.21224.

[7] FBGS.com. (2018) Optical Fibre Bragg Grating sensor technology (FBG). Retrieved December 1, 2018, from http://www.fbgs.com/technology/dtg-technology/

[8] Le Duigou, A., Davies, P., Baley, C. (2011). Environmental impact analysis of the production of Flax Fibres to be used as Composite Material Reinforcement. *J. Journal of biobased materials and bioenergy*. 5: 1-13

[9] La Rosa, A.D., Recca, G., Summerscales, J., Latteri, A., Cozzo, G., Cicala, G. (2014) Bio-based versus traditional polymer composites. A life cycle assessment perspective. *J. Journal of cleaner production*. 74: 135-144

[10] Matos, C., Cristobal Garcia, J., Aurambout, J.P. (2015). Environmental factsheet: Polylactic Acid. *Environmental Sustainability Assessment of Bioeconomy Products and Processes – Progress Report 1*. European Commission. Joint Research Center. 35-38

[11] MRPI Stichting Milieu Relevante Product Informatie. (2012). *data gevel- en dakbekleding*. (In Dutch)

[12] Benelux Bitume, VBWAsfalt. (2005). Productie van Steenslag. Economische, milieu, maatschappelijke en technische verwegingen bij de keuze van verhardingsmaterialen. (In Dutch)

[13] Dauguet, M., Mantaux, O., Perry, N., Zhao, Y.F. (2015). Recycling of CFRP for high value applications: Effect of sizing removal and environmental analysis of the Super Critical Fluid Solvolysis. *J. Procedia CIRP*. 29: 734-739

[14] Klijn-Chevaleriasa, M., Javed, S. (2017). The Dutch approach for assessing and reducing environmental impacts of building materials. *J. Building and Environment*. 111: 147-159.

PART 3 Synthesis